HYDROLOGICAL PROCESSES
Hydrol. Process. **29**, 1156–1172 (2015)
Published online 11 June 2014 in Wiley Online Library
(wileyonlinelibrary.com) DOI: 10.1002/hyp.10226

Lithological and hydrological controls on water composition: evaporite dissolution and glacial weathering in the south central Andes of Argentina (33°–34°S)

José Gabriel León[1,2]* and Fernando Luis Pedrozo[3]

[1] *Instituto de Nivología Glaciología y Ciencias Ambientales, Av. Ruiz Leal s/n Pque. Gral. S. Martín, Mendoza, 5500, Argentina*
[2] *Departamento General de Irrigación, España 1776, Mendoza, Mendoza, 5500, Argentina*
[3] *Instituto de Investigaciones en Biodiversidad y Medio Ambiente, Recursos Acuáticos, Quintral 1250, San Carlos de Bariloche, 8400, Argentina*

Abstract:

Lithological and hydrological influence on fluvial physical and chemical erosion was studied in a glacierized sedimentary basin with high evaporite presence. Suspended particulate matter (SPM), total dissolved solids (TDS) and major ion concentrations were analysed for 2 years of different hydrologic condition: (i) 2009–2010, $Q = 100\%$ average; and (ii) 2010–2011, $Q = 60\%$ average. Annual hydrograph was simple regime-type with one peak in summer related to snow melting. The intra-annual SPM and TDS variations were directly and inversely associated to Q, respectively. Snow chemistry showed continental influence ($Na^+/Ca^{2+} = 0.17$), and atmospheric input of TDS was <1% of the total exported flux. River water was highly concentrated in Ca^{2+} and SO_4^{2-} (~4 mmol l^{-1}) and in Na^+ and Cl^- (~3 mmol l^{-1}). Ca^{2+}/SO_4^{2-} and Na^+/Cl^- molar ratios were ~1 and related to Q, directly and inversely, respectively. Major ion relationships suggest that river chemistry is controlled by evaporite (gypsum and halite) dissolution having a summer input from sulfide oxidation and carbonate dissolution, and a winter input from subsurface flow loaded with silicate weathering products. This variation pattern resulted in nearly chemostatic behaviour for Ca^+, Mg^{2+} and SO_4^{2-}, whereas Na^+, Cl^- and SiO_2 concentrations showed to be controlled by dilution/concentration processes.
During the 2009–2010 hydrological year, the fluxes of water, SPM and TDS registered in the snow melting–high Q season were, respectively, 71%, 92% and 67% of the annual total, whereas for equal period in 2010–2011, 56% of water, 86% of SPM and 54% of TDS annual fluxes were registered. The SPM fluxes for 2009–2010 and 2010–2011 were 1.19×10^6 and 0.79×10^6 t $year^{-1}$, whereas TDS fluxes were 0.68×10^6 and 0.55×10^6 t $year^{-1}$, respectively. Export rates for 2009–2010 were 484 t km^2 $year^{-1}$ for SPM and 275 t km^2 $year^{-1}$ for TDS. These rates are higher than those observed in glacierized granite basins and in non-glacierized evaporite basins, suggesting a synergistic effect of lithology and glaciers on physical and chemical erosion. Copyright © 2014 John Wiley & Sons, Ltd.

KEY WORDS hydrochemistry; snowmelt runoff; glacial weathering; gypsum; suspended particulate matter; export rate

Received 11 November 2013; Accepted 17 April 2014

INTRODUCTION

Fluvial denudation has been studied to assess the origins of elements and control processes of natural waters composition (Meybeck, 2003) and to estimate the influence of weathering on global biogeochemical cycles (Gaillardet *et al*., 1999). Among the factors controlling weathering and erosion at basin scale, the lithological composition (Bluth and Kump, 1994) and the hydrologic behaviour (Maher, 2011) have received much attention as its effect can be clearly determined (Kump *et al*., 2000). Because of the significance of silicate weathering in global CO_2 dynamics, rivers draining igneous lithologies have been more extensively studied than others. Although it has been suggested that carbonate weathering plays a short-term role as carbon repository (Lasaga *et al*., 1994), it also has been shown that weathering of sedimentary rocks rich in sulfide and carbonate still have an important role in CO_2 dynamics over both short time (Liu and Zhao, 2000) and geological timescale (Torres *et al*., 2014).

The significance of mountains as freshwater sources to lowland areas, particularly in arid and semi-arid regions (Viviroli *et al*., 2007), has gained particular importance in the last decades among the scientific community and water management organizations. Nevertheless, efforts have mainly been focused on assessing the effects of climate change on river discharge (Urrutia and Vuille, 2009; Immerzeel *et al*., 2010), and there is a lack of studies on the effects of hydrological changes on the chemical composition of mountain water resources (Viviroli *et al*., 2011). Given that climate projections

*Correspondence to: José Gabriel León, Instituto de Nivología Glaciología y Ciencias Ambientales, Av. Ruiz Leal s/n Pque. Gral. S. Martín, Mendoza, 5500, Argentina.
E-mail: leondecba@yahoo.com.ar

indicate a regional precipitation decrease of 35% for the end of the 21st century (Vicuña *et al*., 2010), it is reasonable to suggest that changes in the flux and composition of dissolved and particulate loads in rivers will take place in response to discharge decrease scenarios (Godsey *et al*., 2013).

In the Central Andes of Southern South America, watercourses are mainly fed by snow precipitation derived from the moisture carried from the Pacific Ocean by west winds (Masiokas *et al*., 2010). In the eastern watershed of this mountain range, the arid climate strengthens the bond between socio-economic development and water resources, limiting most of human activities to the availability of water resources, which are used for domestic consumption, irrigation, hydroelectrical power generation and industries (Masiokas *et al*., 2006). The regional importance of these hydrological systems has promoted the study of the processes controlling the temporal distribution and amount of runoff (Masiokas *et al*., 2010) and its agronomic use (Chambouleyron *et al*., 1993). However, there is little literature on the factors that control the composition of Andean river waters at this latitude, unlike that on basins located north and south of this region (Pedrozo and Bonetto, 1987; Pedrozo and Chillrud, 1998; Smolders *et al*., 2004; Depetris *et al*., 2005).

Among the watercourses rising in the eastern watershed of the Southern Central Andes, Tunuyán River offers a favourable configuration to evaluate physical and chemical factors. High slopes and the action of snow and glaciers in its upper basin (IANIGLA, in press) combine with mixed lithology of abundant evaporite deposits (Ramos *et al*., 2010). Moreover, because the upper basin is virtually free of human activities, the natural characteristics of the river are not affected in any significant way, allowing the exclusion of anthropogenic interference in the processes of physical and chemical weathering analyses. Although these processes have been studied in glacial granitic basins (Anderson, 2007; Hindshaw *et al*., 2011) and in non-glacial evaporite basins (Smolders *et al*., 2004; Négrel *et al*., 2007), there is a lack of studies on fluvial geochemistry from environments in which both characteristics are combined (Tranter, 2011), as is the case of Tunuyán River.

Here, we assess the effect of basin lithology and determine hydrological features in Tunuyán River water composition. We discuss the relative importance of these processes in the context of mountain rivers geochemistry.

MATERIALS AND METHODS

Study area

The active basin output of Tunuyán River was registered at Valle de Uco gauging station (33°46′35.5″S, 69°16′21.1″W). The drained area is 2456 km^2 (1199–6570 m asl), and the annual discharge is 0.91 km^3, resulting in a specific discharge of 382 mm $year^{-1}$. Average height is ~3500 m asl, mean annual temperature is 2.5 °C, and precipitation ranges 400–550 mm $year^{-1}$ of snow-water equivalent (SWE) (DGI, 2011).

This part of the basin comprises a strip stretching 80 km from N to S characterized by steep slopes (~30%) of two parallel mountain ranges: the Principal Cordillera, in the border Argentina–Chile, and the Frontal Cordillera, located eastward. The Principal Cordillera is composed of Miocene volcanic arc rocks, as well as Mesozoic and Paleogene sedimentary and magmatic formations on top of Late Paleozoic/Triassic magmatic sequences, similar to those that comprise the Frontal Cordillera (Kay *et al*., 2004). In Tunuyán basin, the Principal Cordillera is rich in sandstones, carbonates and evaporites, cyclically deposited during the marine transgressions and regressions (Jurassic–Cretaceous) and exposed by Andean orogeny (Table I). The lithology of the Frontal Cordillera comprises black shales, plutonic and metamorphic rocks (Carboniferous–Permian to Triassic) such as granites, migmatites and a smaller proportion of marble rocks (Ramos *et al*., 2010).

Ice glaciers with and without debris cover occupy 60 and 118 km^2, whereas rock glaciers account for 28 km^2 (IANIGLA, in press). The ice forms concentrate at the northern and central parts of the basin (Figure 1). Northern glaciers are located over volcanic rocks and black shales, whereas central glaciers are also over sandstones, carbonates and evaporites.

Tunuyán River is mainly fed by snowmelt and glacier ablation. A strong and direct relationship between winter snowpack and spring–summer river discharges has been observed (Masiokas *et al*., 2010), resulting in a simple regime-type annual hydrograph with a single discharge peak (~70 $m^3 s^{-1}$) in December–January. The intra-annual

Table I. Area of the main lithological units in the study area and glacier cover of each one (Ramos *et al*., 2010; IANIGLA, in press)

	Area		Glacier cover	
Lithology	(km^2)	%	(km^2)	%
Volcanic rocks	726	30	101	14
Granitoids	566	23	16	3
Metamorphic rocks	85	3	7	9
Quaternary deposits	104	4	8	8
Sandstones and conglomerates	297	12	9	3
Black shales and sandstones	198	8	21	11
Black shales and carbonates	52	2	3	5
Carbonatic sandstones and gypsum	174	7	21	12
Limestones and evaporites	93	4	2	2
Gypsum and evaporites	161	7	19	12

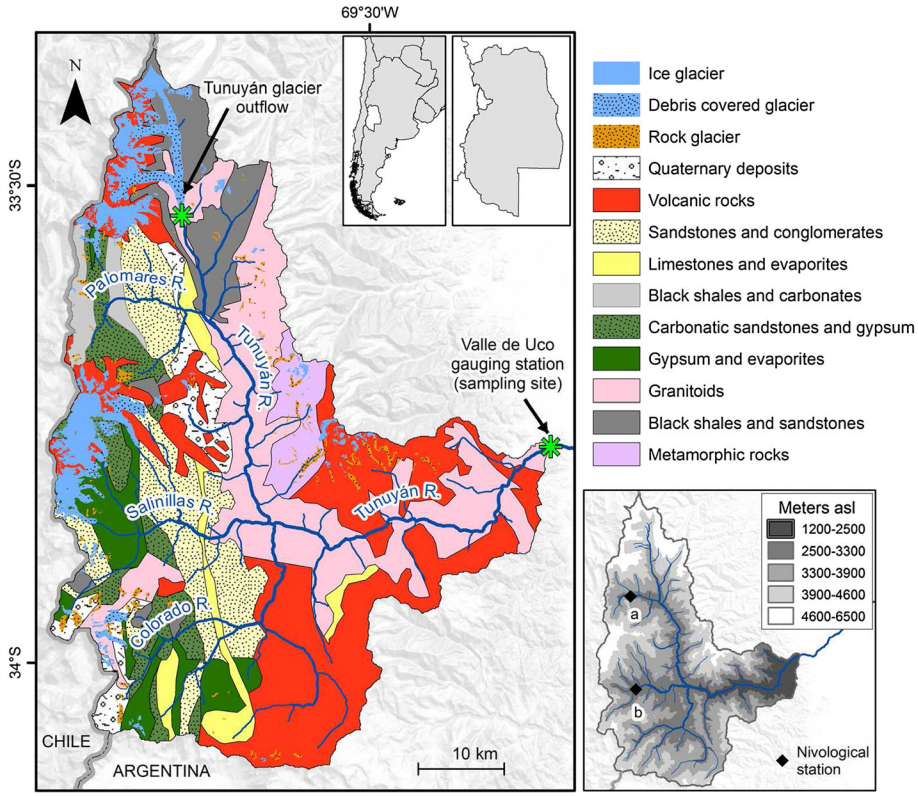

Figure 1. Simplified geological map of Tunuyán River basin (modified from Ramos *et al*., 2010). Glacier mapping is based on data from IANIGLA (in press). Altimetry and nivological stations (a: Palomares station, b: Salinillas station) are also shown

discharge distribution is characterized by a high discharge season from late September to late March and a complementary low discharge season when the runoff is composed primarily of base flow relatively constant at ~13 $m^3 s^{-1}$.

The vegetation in the basin is composed of scattered shrub and cushion-like plants, belonging to the High Andean Phytogeography Province (Roig *et al*., 2007). Direct impact of anthropogenic activities in the basin is low owing to the absence of human settlements, the lack of roads suitable for vehicular traffic, and the remoteness from industrial centres.

At sampling site, water composition results from the mixing of four watercourses draining heterogeneous lithology (Figure 1). The northern part, where Tunuyán River begins, is rich in volcanic rocks and black shales capped by glaciers. The first tributary, Palomares River, is located southward and hosts black shales, carbonatic sandstones and gypsum with glaciers on top of volcanic formations. Downstream, the Salinillas River basin is profuse in limestones, gypsum and evaporitic deposits with glaciers on top. Finally, the Colorado River basin is scarce in glaciers and is divided in a higher half dominated by limestones, carbonatic sandstones, gypsum and evaportites and a lower half with volcanic rocks.

METHODS

The present study ran from March 2009 to March 2011, comprising two hydrological years. River water samples were collected monthly from Tunuyán River (33°45′34″S, 69°12′44″W) at approximately 11:00 AM where we measured *in situ*: temperature (Temp), pH (Thermo-Orion 230A); electrical conductivity (EC) automatic temperature compensation at 25 °C (WTW Multiline P4); and dissolved oxygen (DO) (Thermo-Orion Star3). The samples for determining suspended particulate matter (SPM) concentration were collected in wide-mouth 1-l flasks; the samples for determining the concentrations of total dissolved solids (TDS) and major ions (Ca^{2+}, Mg^{2+}, Na^+, K^+, HCO_3^-, SO_4^{2-} and Cl^-) were collected in 1.5-l PVC bottles. All containers were rinsed three times with river water before sample collection and taken to the laboratory refrigerated in the dark. Samples were filtered within 4 h after collection (0.45 µm, cellulose acetate) and analysed within 24 h. SPM was determined by the difference in mass on GF/F filters previously pre-calcined at 500 °C for 4 h and weighed, by filtering variable volumes of water (30–1000 ml) up to filter clogging, which were then dried to constant mass at 60 °C. TDS concentration was estimated in filtered water evaporated at 180 °C; Ca^{2+} and Mg^{2+} by titration with EDTA, Na^+ and K^+ by flame photometry HCO_3^- by titration with H_2SO_4

(0.02 N) in unfiltered water, SO_4^{2-} by gravimetry with barium chloride, Cl^- by the argentometric method and soluble reactive silica (SiO_2) by the silicomolybdate method. SiO_2 concentration was determined in five samples ($N=5$) collected during the falling limb of the hydrograph (December to March) for year 2010–2011. All the analyses were performed in compliance with APHA (1998). Standard error for duplicate analysis was <3%. Charge balance error was $-0.8 \pm 1.7\%$ ($N=22$).

The mineralogical composition of SPM at the sampling site in August 2009 (low discharge season) was determined by X-ray diffraction pattern analysis (Philips PW 1701/01 Cu-K_α radiation at 40 kV and 30 mA, 2θ range 5–65°, 0.03° step size. CNEA, S.C. Bariloche). The saturation indexes of the main minerals were calculated with Visual MINTEQ 3.0 (Gustafsson, 2010).

The mean daily discharge of Tunuyán River is routinely measured by the Argentine Secretariat for Water Resources (SRH, 2013) at 7 km upstream from the sampling site (Figure 1). The meteorological data of the upper basin – mean daily air temperature, daily incident solar radiation and SWE – were obtained from two stations located within the Upper Tunuyán River Basin (Palomares and Salinillas at 3080 and 2615 m asl, respectively) and at Laguna del Diamante located at 4 km south (3334 m asl). The three stations have time series data of over 10 years. The water volume resulting from snow precipitation was estimated to be the product of the snow cover area by the average SWE values. The snow cover area was determined by MODIS/Terra images (Hall *et al.*, 2011) taken on the date on which the maximum SWE was recorded. In September 2010 and 2011, and in August 2012, nine snow samples were collected in the region (32°47′–35°08′S), and one water sample was taken at Tunuyán glacier outflow (Figure 1) in February 2013. In these samples, dissolved Ca^{2+}, Mg^{2+}, Na^+, K^+ and Si were determined (ICP-MS Agilent Technologies Series 7500 cx. ISIDSA–Universidad Nacional de Córdoba). Snow was first melted at room temperature to measure pH and EC and then filtered through 0.22-μm pore cellulose acetate filters and acidified with HNO_3 (Merck SupraPur®). In addition, dissolved SO_4^{2-} and SiO_2 were determined in the glacier outflow sample by turbidimetric and molybdosilicate methods, respectively (APHA, 1998).

The atmospheric input of dissolved solids was estimated as the product of cation and anion concentrations by the volume of water precipitation. For the purpose of this estimate, cation concentration was calculated as the average of all analysed samples, and anion concentration was the anion value in the precipitation from Pedrozo *et al.* (1993).

The annual loads (L_i) of SPM, TDS, cations and anions in Tunuyán River were calculated as follows:

$$L_i \sum_{i=1}^{n} C_i Q_i$$

where n is the number of days in the year; C_i is the daily concentration of i component, estimated by linear interpolation between the values in the time series (Ollivier *et al.*, 2010); and Q_i is the mean daily discharge.

It has been demonstrated that, in low-frequency sampling, the high variability in [SPM] concentration during high discharge periods can lead to underestimation of flux (Skarbøvik *et al.*, 2012). Therefore, a complementary data set of SPM concentration supplied by the SRH (2013) was used. This data set comprised the same study period but with a weekly frequency during the snow-melting season, which has been shown to increase the precision in SPM annual flux estimation (Moatar and Meybeck, 2005). The SRH database (2013) ($N=54$) was compared with the one obtained in the present study ($N=22$) without obtaining significant differences (Figure 3).

Correlations between hydrological, meteorological and chemical variables were determined with Spearman rank order coefficient (R_S) (Négrel *et al.*, 2007).

RESULTS

The meteorological variables in the Upper Tunuyán River Basin (2600–3600 m asl) had a distinctive seasonal pattern. Daily incident solar radiation (6.6–30.6 MJ m^{-2} day^{-1}) and temperature (−15–14 °C) were directly correlated and inversely associated with snow accumulation (Figure 2). The maximum snow accumulation during the winter of 2009 was 437 mm SWE (1956–2011 average = 484 mm SWE), whereas winter 2010 precipitations accounted for 126 mm SWE, one of the lowest records in the last six decades (SRH, 2013).

The mean annual discharge of Tunuyán River during hydrologic year 2009–2010 was 28.9 m^3 s^{-1}, similar to the value (28.8 m^3 s^{-1}) in the 1954–2011 series (SRH, 2013), whereas during year 2010–2011, this value was 17.4 m^3 s^{-1}, 60% of the historical value (Table II) owing to snow scarcity in year 2010 (Figure 2). The annual hydrograph of Tunuyán River is typical of snowmelt-fed rivers, with only one maximum in summer and the minimum in winter (De Walle and Rango, 2008). The amplitude of the daily hydrograph during the snow-melting season was up to 30% of the mean daily discharge (Q) between maximum and minimum hourly discharge (Figure 3). Therefore, with the purpose of comparing the discharge at the time of sampling collection with Q, the difference between the latter (average of 24 hourly measurements) and the mean discharge at 11:00 (average of 3600 secondly measurements) was

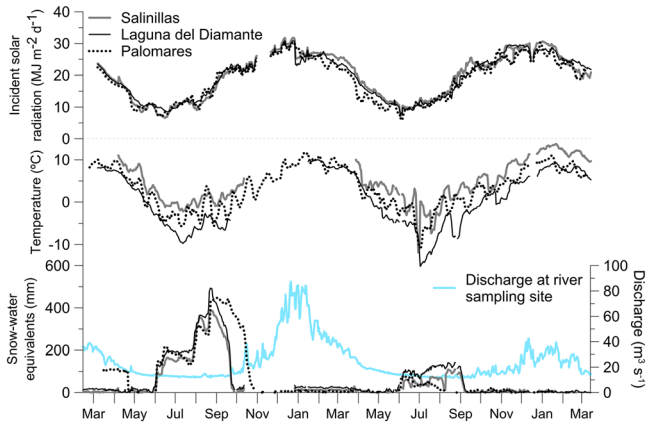

Figure 2. Incident solar radiation, temperature and snow-water equivalent at nivological stations in the high catchment of Tunuyán River from 2009 to 2011. River discharge at sampling site is also shown

Table II. Annual discharge, average daily discharge and standard deviation (SD) in Tunuyán River (Valle de Uco gauging station: 33°46′35.5″S, 69°16′21.1″W) for different periods

Period	Annual discharge (hm^3)	Mean daily discharge ($m^3 s^{-1}$)	SD
1954–2011	909	28.9	19.2
2009–2010	913	28.7	20.3
2010–2011	536	**20.3**	8.6

Mean daily discharge for 2010–2011 period (in bold) was significantly different to historical mean (1954–2011) and 2009–2010 periods (Kruskal–Wallis. $H = 10.2$, $p < 0.01$, $N = 365$).

calculated for each sampling date. In all cases, the difference between Q and the average discharge at 11:00 AM was below ±5%.

As observed with Q, the water temperature in Tunuyán River had a characteristic seasonal pattern (Table III). Water temperature reached minimum values (~2 °C) in winter and increased at the beginning of the snow-melting season (~11 °C) but decreased during the hydrograph peak (~10 °C) and increased once again by the end of the higher Q phase (~11 °C). This pattern may be due to the influence of snowmelt cold water. At the beginning of the snow-melting season, water temperature increases until ambient temperature is not high enough to sustain the increase in the temperature of the cold meltwater mass, thus, staying cold during the Q peak. When the volume of meltwater decreases and the ambient temperature is still high, the river temperature increases once again.

The pH was alkaline (7.9–8.6), and although it did not show seasonality, the lowest values were registered at high Q and low TDS, whereas the highest pH levels were observed during the low Q season and low-concentrated waters. DO concentration was always over 8.0 $mgO_2 l^{-1}$, and the peaks coincided with the lower water temperature seasons (~12.0 $mgO_2 l^{-1}$/~2 °C).

The average SPM concentration was 984 $mg l^{-1}$ (28–6470 $mg l^{-1}$), whereas TDS concentration was 864 $mg l^{-1}$ (633–1092 $mg l^{-1}$). These variables were highly dependent on Q (Figures 3 and 5). Two intra-annual periods could be observed: (i) low Q, from late autumn to

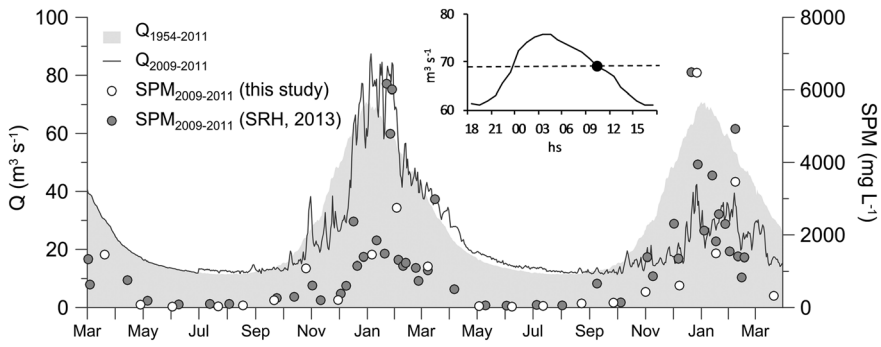

Figure 3. Average daily discharge (Q) and concentration of suspended particulate matter (SPM) in Tunuyán River. Historical average discharge (1954–2011) is also shown. SPM values include SRH (2013) database. The inset shows a daily cycle of discharge variation during the period of maximum runoff (6 January 2010). The black circle indicates the instantaneous discharge at the time of sample collection, and the dotted line represents the average daily discharge

Table III. Average daily discharge (Q) and physical and chemical characteristics of Tunuyán River at Valle de Uco gauging station and Tunuyán Glacier outflow (Figure 1)

Date	Q ($m^3\,s^{-1}$)	Temp. (°C)	pH	DO ($mgO_2\,l^{-1}$)	EC ($\mu S\,cm^{-1}$)	SPM ($mg\,l^{-1}$)	TDS ($mg\,l^{-1}$)	Ca^{2+} ($mmol\,l^{-1}$)	Mg^{2+} ($mmol\,l^{-1}$)	Na^{+} ($mmol\,l^{-1}$)	K^{+} ($mmol\,l^{-1}$)	SO_4^{2-} ($mmol\,l^{-1}$)	HCO_3^{-} ($mmol\,l^{-1}$)	Cl^{-} ($mmol\,l^{-1}$)	SiO_2 ($mmol\,l^{-1}$)
20 March 2009	33	9.5	8.3	9.9	749	1457	747	3.57	0.82	2.61	0.05	3.52	1.66	2.26	—
28 April 2009	18	8.5	8.3	10.1	780	80	781	3.32	0.58	3.05	0.10	3.51	1.67	2.62	—
02 June 2009	13	6.7	8.4	10.5	1200	29	923	4.37	0.74	3.52	0.20	4.10	2.10	3.30	—
22 July 2009	12	2.3	8.4	11.5	1150	32	887	4.24	0.33	3.61	0.15	4.04	2.08	3.67	—
18 August 2009	13	4.5	8.2	11.0	1140	62	996	4.44	0.91	3.74	0.13	4.11	2.05	4.18	—
21 September 2009	14	9.7	8.6	9.9	1197	205	877	4.14	0.78	3.57	0.10	3.77	1.92	3.47	—
26 October 2009	19	10.6	8.3	9.7	978	1086	790	3.37	0.78	2.96	0.08	3.62	1.92	2.12	—
30 November 2009	26	9.7	8.4	9.9	1031	212	758	3.52	0.70	2.61	0.08	3.67	1.69	2.23	—
06 January 2010	81	9.7	8.2	10.5	810	1456	680	3.37	0.74	1.61	0.05	3.75	1.21	1.44	—
02 February 2010	68	10.0	8.3	10.0	757	2751	633	3.24	0.70	1.74	0.05	3.76	1.08	1.44	—
08 March 2010	42	11.2	8.2	8.3	870	1135	657	3.37	0.45	1.91	0.05	3.45	1.25	1.58	—
03 May 2010	19	9.4	8.5	10.0	1473	42	971	4.72	0.37	3.74	0.08	4.35	1.93	3.58	—
08 June 2010	14	5.1	8.6	10.8	1695	28	991	4.27	0.82	4.09	0.10	4.29	2.05	3.92	—
12 July 2010	12	1.7	8.3	11.8	1597	48	1049	4.57	0.62	4.44	0.15	4.46	2.15	4.68	—
23 August 2010	12	7.2	8.4	10.0	1565	116	1092	4.89	0.45	4.65	0.10	4.32	1.97	4.82	—
27 September 2010	13	10.0	8.4	9.61	1626	132	1041	4.92	0.37	4.83	0.08	4.37	2.00	4.99	—
01 November 2010	14	12.7	8.4	9.6	1451	430	1073	4.54	0.53	5.13	0.08	4.51	1.77	4.51	—
08 December 2010	18	13.0	8.0	9.3	1278	606	946	4.14	0.66	3.57	0.08	4.29	1.56	3.10	0.22
27 December 2010	37	12.3	7.9	9.7	1016	6470	749	3.87	0.37	1.83	0.08	3.98	1.29	1.83	0.13
17 January 2011	23	11.4	8.5	9.5	1080	1489	761	3.69	0.25	2.39	0.08	3.77	1.44	2.40	0.18
07 February 2011	31	12.6	8.1	9.2	959	3463	705	3.52	0.62	1.83	0.05	3.70	1.29	1.66	0.13
21 March 2011	16	12.5	8.3	9.3	1210	327	891	4.02	0.74	3.39	0.05	3.97	1.56	3.95	0.23
Tunuyán Glacier Feb-2013	—	—	7.8	—	616	—	487	1.77	0.69	0.39	0.05	2.37	—		0.19

early spring showing minimum SPM and maximum TDS concentrations; and (ii) high Q from late spring to early autumn, of diluted waters with high SPM concentration. There was no apparent intra-annual hysteresis behaviour between these variables and Q.

During the 2009–2011 period, SPM and Q were directly associated fitting an empirical power law, while TDS concentration was inversely related to Q fitting also an empirical power law (Figure 5), showing the typical dilution/concentration pattern of snowmelt-fed rivers (Willis, 2011).

Tunuyán River water was highly mineralized and of calcium sulfate type. The sum of major cations (ΣZ^+) varied between 9.6 and 15.5 meq l^{-1}, and the average concentration of SiO_2 was 0.18 mmol l^{-1} ($N = 5$). The relative composition of major anions (ΣZ^-) and cations (ΣZ^+) was as follows:

ΣZ^+: $Ca^{2+} = 59–70\%$, $Na^+ = 16–33\%$, $Mg^{2+} = 5–15\%$, $K^+ = <1–2\%$

ΣZ^-: $SO_4^{2-} = 56–75\%$, $Cl^- = 14–2\%$ and $HCO_3^- = 11–17\%$.

TDS concentration was positively associated with the concentrations of Cl^-, Na^+, Ca^{2+} and SO_4^{2-} having R_S values of 0.95, 0.92, 0.90 and 0.86, respectively ($N = 22$, $p < 0.0001$). Also, significantly positive associations were observed for HCO_3^- and K^+ concentrations showing R_S values of 0.78 and 0.63, respectively ($N = 22$, $p < 0.05$). Concentrations of major ions and silica were negatively correlated to Q: major ions, $R_S = -0.92$ to -0.71, $p < 0.01$, $N = 22$; and SiO_2, $R_S = -0.97$, $p < 0.001$, $N = 5$.

The average pH of snow water was 6.1 (Table IV), which is higher than the expected level for CO_2 dissolution in distilled water (pH: 5.6). The average conductivity was low (~11 µS cm^{-1}) with a predominance of Ca^{2+} concentrations (79–91% of ΣZ^+) over Na^+ concentrations (5–13% of ΣZ^+). Concentration of Si in all snow samples was below detection limit (<0.46 µmol l^{-1}).

Ionic ratios in river water were calculated from uncorrected concentration because atmospheric precipitation supplied a negligible dissolved mass to the exported fluxes (<1%, Table VII). River waters showed more variable Na^+ (1.6–5.1 mM) and Cl^- (1.4–5.0 mM) concentrations than those of Ca^{2+} (3.2–4.9 mM), SO_4^{2-} (3.4–4.5 mM) and HCO_3^- (1.1–2.1 mM). The co-variation of Na^+ and Cl^- was closely related to theoretical line of halite dissolution ($Na^+ = Cl^-$) having an average Na^+/Cl^- value of 1.1 ± 0.1 (Figure 7A). Likewise, the Ca^{2+}/SO_4^{2-} ratio had an average value of 1.0 ± 0.1 (Figure 7B), but it diverged from the theoretical line of gypsum dissolution ($Ca^{2+} = SO_4^{2-}$) towards the extreme values of the hydrograph, resulting in an excess of SO_4^{2-} during the peak discharge and of Ca^{2+} in the wintertime base flow (Figure 7B). The concentrations of Ca^{2+} and of HCO_3^- (Figure 7C) were correlated ($R = 0.72$; $p < 0.05$) but differed from the theoretical pattern of calcite dissolution showing excess of Ca^{2+} ($Ca^{2+}/[½\ HCO_3^-] = 3.2 \pm 0.4$). Calcium to sulfate and sodium to chloride ratios were related with Q fitting to an empirical power law (Ca^{2+}/SO_4^{2-}: $R_S = -0.78$, $p < 0.001$; Na^+/Cl^-: $R_S = 0.70$, $p < 0.001$). Major ions daily fluxes (Figure 8) reflected the observed ionic ratios (Figure 7). Although the flux pattern was close to the expected for halite and gypsum dissolution ($Na^+ = Cl^-$, $Ca^{2+} = SO_4^{2-}$), during most of the year, Na^+ was higher than Cl^-, whereas SO_4^{2-} was higher than Ca^{2+} only during the hydrograph peak, when the higher fluxes values are recorded.

Table IV. Major dissolved cations in snow from Andes in Mendoza Province (32°42′- 35°17′S) and in precipitation of the Andes in San Juan Province (Lecomte *et al.*, 2008), Patagonian Andes (Pedrozo *et al.*, 1993) and the overall range of continental and coastal rain (Langmuir, 1997)

Site	Elevation (m asl)	Date	pH	EC	Ca^{2+}	Mg^{2+}	Na^+	K^+
				(µS cm^{-1})	(µmol l^{-1})			
Snow Andes Mendoza								
32°44′S–70°06′W	3500	Sept 2011	5.6	4	13.8	1.2	0.5	0.4
34°47′S–69°56′W	3050	Sept 2011	6.9	15	48.7	2.2	1.4	0.4
33°14′S–69°38′W	3800	Sept 2010	6.9	12	38.0	4.5	13.0	2.3
33°14′S–69°38′W	3800	Sept 2011	6	11	39.0	5.6	5.8	1.7
34°07′S–69°42′W	3300	Sept 2010	—	27	110.9	3.2	11.7	2.8
34°28′S–70°01′W	3600	Sept 2010	—	8	11.8	0.9	7.0	2.4
35°08′S–70°12′W	2250	Sept 2010	—	7	22.7	1.4	5.6	1.4
35°08′S–70°12′W	2250	Sept 2011	5.7	3	9.3	0.7	0.1	9.8
35°08′S–70°12′W	2250	Aug 2012	5.2	8	11.3	1.0	1.2	0.3
Snow Andes San Juan (30°S)			6.5	13	17.5	2.1	38.3	15.9
Rain Andes Patagonia (41°S)			5.1		3.0	0.5	2.8	0.6
Continental rain range			4–6		3.0–80.1	2.1–20.2	9.1–40.0	3.1–8.0
Coastal rain range			5–6		5.0–39.9	16.1–60.1	40.0–200.1	5.1–15.1

Suspended particulate matter mineralogy is summarized in Table V. Plagioclase dominated the mineralogical composition (44%) followed by K-feldspar (15%). Quartz, mica and clays accounted for 15% and carbonates and sulfates for 7% and 3%, respectively. This distribution was related with basin lithology (Table I), where basalt, andesite and granitoid dominated the area (53%) followed by black shale and sandstone (22%) and carbonate and evaporite (17%).

The calculated saturation indexes (SI) (Figure 4) showed that the Tunuyán River waters were oversaturated with respect to quartz (SiO_2: $SI_{qrz} = 0.36–1.11$) and to calcite ($CaCO_3$: $SI_{cal} = 0.19–1.03$) and under-saturated with respect to evaporite minerals such as gypsum ($CaSO_4$: $SI_{gyp} = -0.72$ to -0.92) and halite (NaCl: $SI_{hal} = -7.71$ to -6.26). Dolomite SI fluctuated throughout the year ($CaMg[CO_3]_2$: $SI_{dol} = -1.28–0.64$), showing an oversaturation at pH values >8.3.

Table VI summarizes the concentrations of the variables considered during the hydrological years studied. Coinciding with the lower discharge in 2010–2011, TDS concentration showed higher values during that period than throughout 2009–2010, when runoff was higher. In addition, although the mean SPM concentration was not significantly different between years, a 50% increase and a wider variation range were observed during 2010–2011. Also, the associations between *Q* and SPM and between *Q* and TDS showed a stronger relationship when considering the water years separately than when considering them as a single period (Figure 5).

Table V. Mineral species identified by X-ray diffraction in the suspended solids from Tunuyán River and semi quantitative content values

Compound name	Mineral group	Content (%)	Chemical formula
Quartz	Quartz	3	SiO_2
Muscovite	Mica	9	$K_{0.96}Al_{1.88}(Si_3Al)_{0.955}O_{10}$ $((OH)_{1.8}O_{0.2})$
Biotite	Mica	1	$KFeMg_2(AlSi_3O_{10})(OH)_2$
Kaolinite	Clay	2	$Al_4(OH)_8$ (Si_4O_{10})
Illite-montmorillonite	Clay	3	$KAl_4(Si,Al)_8O_{10}(OH)_4{\cdot}4$ H_2O
Orthoclase	K-feldspar	9	$K(AlSi_3)O_8$
Microcline	K-feldspar	6	$K(AlSi_3)O_8$
Albite	Plagioclase	7	$Na(AlSi_3O_8)$
Andesine	Plagioclase	8	$Na_{0.685}Ca_{0.347}$ $(Al_{1.46}Si_{2.54}O_8)$
Labradorite	Plagioclase	10	$Ca_{0.64}$ $Na_{0.35}$ $(Al_{1.63}Si_{2.37}O_8)$
Bytownite	Plagioclase	7	$Ca_{0.86}Na_{0.14}$ $(Al_{1.94}$ $Si_{2.06}O_8)$
Anorthite	Plagioclase	12	$Ca(Al_2Si_2$ $O_8)$
Forsterite	Olivine	2	Mg_2SiO_4
Pyroxene	Pyroxene	7	$Mg_2Si_2O_6$
Diopside	Pyroxene	2	$Ca(Mg,Al)(Si,Al)_2O_6$
Hydroxylapatite	Carbonate	2	$Ca_5(PO_4)_3$ (OH)
Calcite, magnesian	Carbonate	2	$Mg_{0.1}Ca_{0.9}CO_3$
Calcium Carbonate	Carbonate	3	$CaCO_3$
Epsomite	Sulfate	3	$MgSO_4$ $(H_2O)_7$
Gibbsite	Hydroxide	1	$Al(OH)_3$

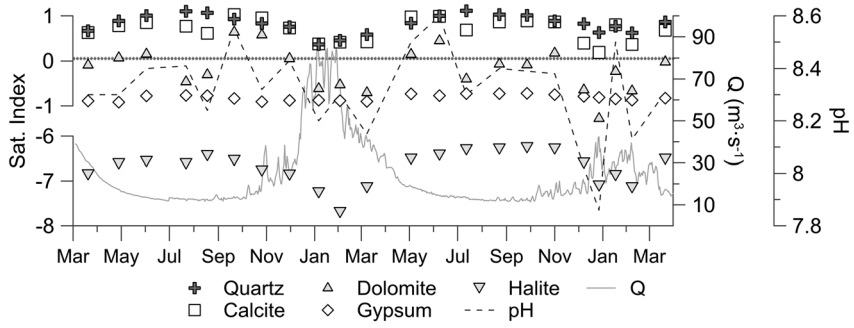

Figure 4. Saturation indices of quartz, calcite, dolomite, gypsum and halite in Tunuyán River from 2009 to 2011. pH and average daily discharge (*Q*) are also shown

Table VI. Mean concentrations of suspended particulate matter (SPM), total dissolved solids (TDS) and major ions in Tunuyán River for 2009–2010 year (discharge = 100% historical average) and 2010–2011 year (discharge = 60% historical average)

	SPM		TDS		Ca^{2+}		Mg^{2+}		Na^{+}		K^{+}		SO_4^{2-}		HCO_3^{-}		Cl^{-}	
Period	($mg\,l^{-1}$)				($mmol\,l^{-1}$)													
2009–2010	773	a	794	a	3.72	a	0.70	a	2.74	a	0.10	a	3.76	a	1.69	a	2.54	a
2010–2011	1196	a	934	b	4.29	b	0.53	a	3.61	b	0.08	a	4.19	b	1.72	a	3.58	b

Different letters indicate significant differences between the considered hydrological years (Wilcoxon matched-pairs test, $p < 0.05$, $N = 11$).

The estimated annual SPM load was 1.19×10^6 t for 2009–2010 and 0.79×10^6 t for 2010–2011 (Table VII), occurring 92% and 86% during the high Q period. For the same interval, the TDS loads were 0.67×10^6 and 0.53×10^6 t. The temporal distribution of TDS load had a similar pattern to that of the SPM but less pronounced: 67% and 54% of the annual mass of dissolved matter were registered during the snow-melting season of the periods 2009–2010 and 2010–2011, respectively. For the same periods, atmospheric inputs of dissolved matter were estimated to be 4780 and 606 t, representing 0.71% and 0.11%, respectively, of total river export.

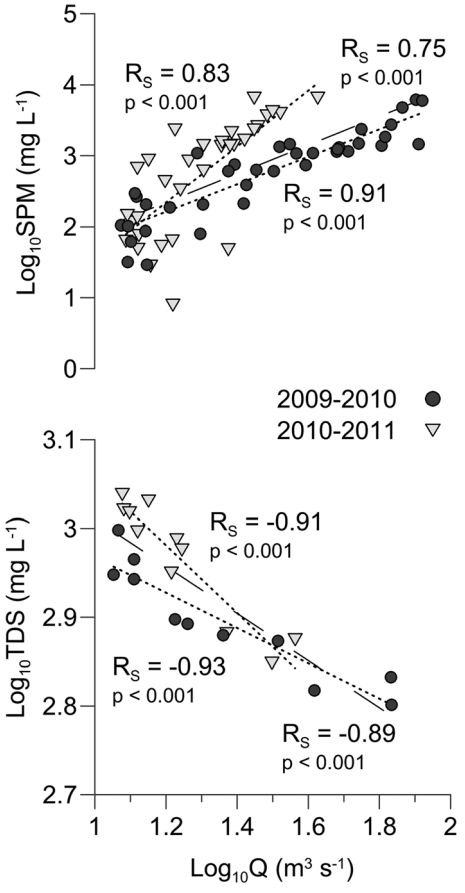

Figure 5. Relationships of suspended particulate matter (SPM) and total dissolved solids (TDS) with discharge (Q) in Tunuyán River for 2009–2010 (annual discharge = 100% of historical average) and 2010–2011 (annual discharge = 60% of historical average) hydrological years. The SPM data set includes values of SRH (2013). R_S: Spearman rank order correlation coefficient. Dotted lines represent *log–log* regression lines for the 2009–2010 and 2010–2011 years and dashed lines for the 2009–2011 period

DISCUSSION

Hydrology

Incident radiant energy is an important factor controlling the hydrologic cycle of snowmelt rivers (De Walle and Rango, 2008). In the Upper Tunuyán River basin, incident solar radiation values during the snow-melting period were 26 MJ m^{-2} day^{-1}, similar to those measured by Schrott (1998) in the Agua Negra Stream basin (~21 MJ m^{-2} day^{-1}), located 400 km northward at 4500 m asl. These values are characteristic of mountainous regions at mid-latitudes and are caused by high solar elevation as well as lower absorption by clouds and atmospheric constituents (Barry and Chorley, 2010). In arid regions, inter-annual variability of precipitations reaches values close to 100% (Simmers, 2003). In a recent study, Masiokas *et al.* (2010) analysed snow records and river discharges in the Andes (30°–37°S) in the period 1951–2008 and observed a greater inter-annual variability in snow records than in river discharges. The most extreme case was registered in 1968, when snowfall and river discharges in the region were 6% and 50%, respectively, of the historical average. During the 2009–2010 period, snow precipitations and discharge showed values close to 100% of the historical averages, whereas during the 2010–2011 period, precipitations were 6% and the discharge was 60%. This gap in discharge response to precipitations is probably related to groundwater hydraulic dynamics in which residence times that regulate the base flow are higher than those of surface runoff (McDonnell *et al.*, 2010). In South Central Andes, it was observed that in dry years (pp ~ 50%) preceded by wet periods (precipitations 150% of the historical average), the discharge did not decrease proportionally to the decrease in precipitations (Table VIII). A similar pattern was observed during this study. The snow precipitation volume in the

Table VII. Atmospheric input, river flux and erosion rate of particulate and dissolved matter (SPM, TDS) for 2009–2010 (09–10) and 2010–2011 (10–11) water years in Tunuyán River

	Period	SPM	TDS	Ca^{2+}	Mg^{2+}	Na^{+}	K^{+}	SO_4^{2-}	HCO_3^{-}	Cl^{-}	SiO_2
Atmospheric input		10^3 t year^{-1}					10^7 mol year^{-1}				
	09–10	—	4.8	3.22	0.22	0.55	0.23	1.10	3.16	0.68	—
	10–11	—	0.6	0.41	0.03	0.07	0.03	0.14	0.40	0.09	—
River flux		10^3 t year^{-1}					10^9 mol year^{-1}				
	09–10	1189.4	676.2	3.23	0.62	2.18	0.07	3.39	1.38	1.93	0.16
	10–11	789.7	552.8	2.57	0.32	2.08	0.05	2.52	1.03	2.02	0.15
Erosion rate		t km^{-2} year^{-1}					10^6 mol km^{-2} year^{-1}				
	09–10	484.3	275.3	1.32	0.25	0.87	0.03	1.38	0.56	0.79	0.07
	10–11	321.5	225.1	1.05	0.13	0.85	0.02	1.03	0.42	0.82	0.06

Erosion rate is corrected for atmospheric input. For the calculation of SiO_2 transport (see text), concentration was estimated by the empirical relationship $SiO_2 = 102.85\ Q^{-0.72}$, $R = 0.97$, $p < 0.001$, $N = 5$ (Clow and Mast, 2010).

Table VIII. Regional snowpack in central Andes (Masiokas *et al*., 2006) and annual discharge of Tunuyán River (DGI, 2011) for the driest years of 1950–2011 period

	Precipitation	Annual discharge
Year	% historical average	
1968	6	57
1996	19	56
2010	24	59
2004	28	69
1985[a]	29	98
1998	29	69
1990	39	73
1967	43	73
1956	45	63
1964	49	66
1973[a]	52	110

Values are expressed as % of the 1951–2011 average.
[a] Annual average precipitation in the previous year >170%.

Tunuyán River drainage basin in 2009–2010 was estimated to be 946 hm^3, and the total annual discharge measured was 912 hm^3; whereas in the 2010–2011 period, these were 120 and 536 hm^3, respectively, i.e. during the dry year, 78% of river discharge would come from groundwater deposits.

Precipitation correction

Given the marine origin of the moisture feeding the rivers draining South Central Andes (Masiokas *et al*., 2010), cyclic salt content in precipitations could influence the estimation of flux and weathering rates. In Argentina, Drago and Quirós (1996) observed that the influence of marine aerosols on the chemistry of precipitations is only significant in coastal regions. In Andean Rivers, this marine influence is well documented (Table IV). Lecomte *et al*. (2008) studied the hyperarid Agua Negra Stream basin (~30°S, ~4000 m asl), located at 160 km from the ocean. These authors found Na^+/Ca^{2+} ratios ~2.40 in snow samples and estimated that all Cl^- and part of Na^+ transported by that stream originate from marine aerosols. Hoke *et al*. (2013) analysed δD and $\delta^{18}O$ from river, snow and ice waters in a transect through the Andes (~70° 50′ to ~68°50′W at ~33°S, 827 to 3200 m asl) and established the westerly Pacific origin of precipitation on the eastern slopes at elevations above 2 km. In Patagonian Andes (~41°S, ~2000 m asl), at 170 km from the ocean, Pedrozo *et al*. (1993) recorded low salinity in precipitations with low levels of Na^+ and pointed out that the little marine influence is related to the distance from the ocean and to the orogenic effect of the Andes, which promote cation strip-out in the windward (western) side. Finally, our results showed that the oceanic effect in the chemical composition of snow precipitations in the eastern side of the Andes (32°–36°S, 2300 to 3800 m asl) would be minor given the low Na^+ concentration (~6 μM) and Na^+/Ca^{2+} values (~0.17) registered in snow samples. The predominance of Na^+ over Ca^{2+} ($Na^+/Ca^{2+} > 5$, molar) in snow chemistry had been considered to indicate marine influence, whereas Ca^{2+} enrichment at low Na^+ concentrations (<100 μmol l^{-1}) would come from non-sea salt Ca^{2+} from dust (Krnavek *et al*., 2012).

A possible driver of marine influence on Andes snow chemistry is related to the climatic circulation patterns that are responsible for the type of hydrologic year (dry, average or wet). Given that intense storm frequency is higher in wet years (Viale and Nuñez, 2011), the marine influence plume could be extended eastward during these periods. The examination of the sampling dates of the

cited papers reveals a possible support for this hypothesis. Samples with a stronger oceanic signal were collected during wet years, whereas samples showing continental influence were taken during dry periods. Lecomte *et al.* (2008) analysed snow samples obtained in the 2002–2003 water year, which had higher precipitations than the historical average (166%). Hoke *et al.* (2013) sampled snow in Mendoza River during 2008 (126%) and river water from 2001–2002 and 2006–2007 years (151% and 147%, respectively). On the other hand, the samples obtained by Pedrozo *et al.* (1993) corresponded to relatively dry years (77–81%), as the ones in the present study (24–77%), and both showed low salinity and Na^+ content. This pattern could be an indication of the influence of the hydrological year type on the solute content in western South Central Andes precipitations.

Controls on water chemistry

The high mineralization of the Tunuyán River waters (TDS ~900 mg l^{-1}; ΣZ^+ ~12 meq l^{-1}) ranks it among the rivers with the highest saline concentration at global scale (Meybeck, 2003). The high content of SO_4^{2-} and alkaline pH indicate the influence of gypsum and carbonate deposits in its basin (Meybeck, 1987; Bluth and Kump, 1994; Négrel *et al.*, 2007). In other rivers that rise in the eastern side of the Andes, these characteristic have been observed associated with the presence of this type of marine deposits (Pedrozo and Bonetto, 1987; Smolders *et al.*, 2004; Depetris *et al.*, 2005).

According to the Gibbs criteria for classification of rivers (1970), Tunuyán River falls between two categories: 'Rock Dominance' (R-D) and 'Evaporation Crystallization' (E-C) closer to the latter (Figure 6), as observed by Négrel *et al.* (2007) for Ebro River in Spain. However, it seems unlikely that water composition is influenced by *in situ* evaporation/crystallization (i.e. as observed in Llancanelo saline lake, Figure 6). Despite its high TDS concentration, Tunuyán River Na^+/Ca^{2+} ratios (~0.76) are low for waters exposed to intense evaporation. Moreover, the waters of adjacent basins under equal climatic conditions but in volcanic lithology are diluted (Lecomte *et al.*, 2008). The usual represented end-member for evaporitic rocks influencing the river chemistry is high in salt rock content and therefore is expected to show high Na^+/Ca^{2+} values (Ollivier *et al.*, 2010). However, for Tunuyán River basin lithology, that end-member would not represent the expected ionic ratios for rocks weathering in its catchment because of its higher gypsum/halite ratio. Tunuyán River geochemistry seems to respond to R-D influenced by rocks formed by E-C processes. Saline load and ionic ratios comparable with those of Tunuyán River have been recorded in small (<50 km^2) mono-lithological salt and gypsum marl lithologies (Meybeck, 2003).

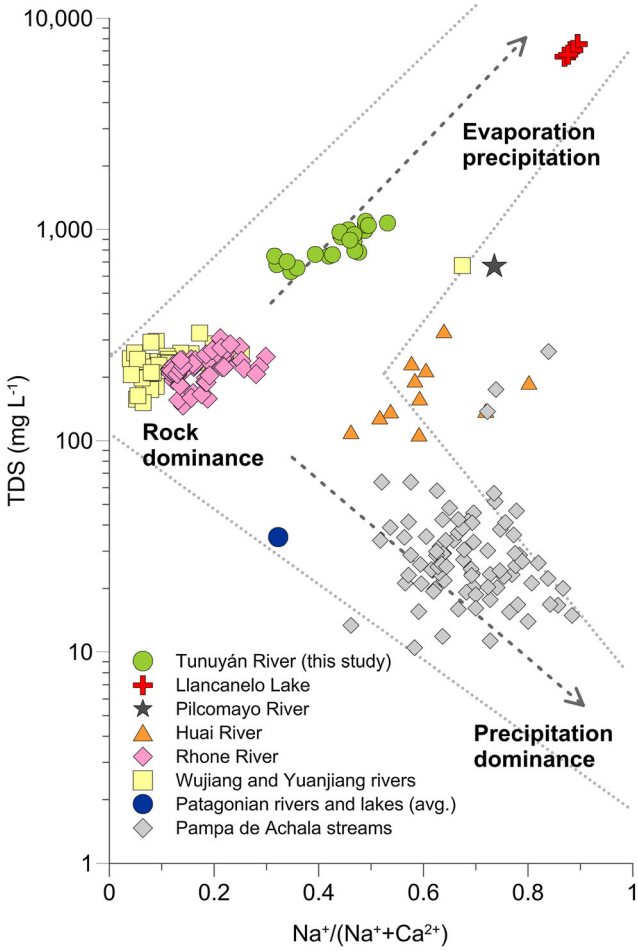

Figure 6. Gibbs diagram (1970) showing Tunuyán River (this study), the Llancanelo salt lake (Manzur *et al.*, 2006), Pilcomayo River (Smolders *et al.*, 2004), Huai River (Zhang *et al.*, 2011), Rhone River (Ollivier *et al.*, 2010), Yaujiang and Wujiang Rivers (Han and Liu, 2004), lakes and rivers of the Andean Patagonia (Pedrozo *et al.*, 1993) and streams from central Argentina (Pampa de Achala) (Lecomte *et al.*, 2011)

The mineral composition of SPM is related with rock type and denudation processes. The dominance of granite and basalt in Tunuyán River basin lithology produces SPM to be dominated by weakly weathered plagioclase, alkali feldspar, mica and clay (Table V). More soluble minerals also present in SPM, such as calcite and epsomite that would result from *in situ* precipitation [e.g. common ion effect (Langmuir, 1997)]. Also, shales of Carboniferous period like the present in high basin have been reported to be rich in calcite, dolomite and pyrite (respectively, 1.4%, 2.1% and 4.3% of dry weight) (O'Brien and Slatt, 1990). It is well known that black shales form on seabed rich in organic matter producing a reducing environment that promotes the formation of pyrite due to the reduction of Fe^{2+} and S^{2-} (Boggs, 2009). These black shales occupy ~10% of the watershed; hence, the importance of this lithology as a source of SO_4^{2-} by pyrite oxidation would be significant.

The high positive correlation between Ca^{2+} and SO_4^{2-} concentrations in river waters (Figure 7B) suggests that gypsum dissolution is an important factor controlling the concentration of these solutes (Smolders *et al.*, 2004). Nevertheless, Ca^{2+}/SO_4^{2-} ratio in Tunuyán River is not steady throughout the year, showing excess of SO_4^{2-} over Ca^{2+} during the hydrograph peak and excess of Ca^{2+} over SO_4^{2-} during the low Q period. Such excess of SO_4^{2-} suggests another origin besides the congruent dissolution of gypsum. Pyrite (FeS_2) oxidation at the bed of glaciers is a known source of SO_4^{2-} (Tranter *et al.*, 2002). This reaction consumes oxygen and is promoted by microorganisms (Montross *et al.*, 2013); thus, the excess of SO_4^{2-} in summer could be due to FeS_2 oxidation favoured by temperature increase and water oxygenation produced by hydraulic movement (Skidmore *et al.*, 2010; Mitchell *et al.*, 2013). In close agreement, the water collected in February 2013 (austral summer) at Tunuyán glacier outflow (Figure 1, Table III) showed a high SO_4^{2-} concentration (2.4 mM) and excess over Ca^{2+} (1.8 mM), and because this ice form is settled mainly over black shales, the outflow composition would indicate the relative importance of sulfide oxidation in sulfate flux control during the summer. Tunuyán glacier outflow drains 169 km^2 (48 km^2 glacier covered), and considering the 2012 winter SWE data (765 mm), an annual input of 124 hm^3 can be roughly estimated, which for a hydrograph equivalent to the one at Valle de Uco gauging station would result in a mean daily discharge of 6.6 $m^3 s^{-1}$ for February, against 32 $m^3 s^{-1}$ and ~350 mg l^{-1} of SO_4^{2-} at Valle de Uco for the same period. According to these values, daily sulfate flux during February at Valle de Uco and at Tunuyán glacier outflow would be 23 224 and 3120 t SO_4^{2-} day^{-1}, respectively. This means that ~13% of the sulfate exported in the basin is supplied by 7% of the area, drawing attention to sulfide oxidation as SO_4^{2-} source during summer. The data of the chemistry of Tunuyán glacier outflow also allow to compare it to runoff chemistry with glaciers from different regions of the world showing the highest concentration values of Ca^{2+}, Mg^{2+} and SO_4^{2-} and the lowest specific runoff (Tranter, 2011).

The apparent excess of Ca^{2+} with respect to SO_4^{2-} in winter (Figure 8) could be due to plagioclase weathering (Drever, 1997) when river discharge is sustained by groundwater, having longer residence times in the subsoil that favours silicate hydrolysis products accumulation (Maher, 2011). The Ca-feldspars are among the most soluble (Meybeck, 2003) and the most abundant silicate mineral in Tunuyán River catchment (Ramos *et al.*, 2010). Also, an increase of Ca^{2+} from carbonate during winter could be expected as these minerals become slightly more soluble at lower temperatures (Stallard, 1995).

The Mg^{2+} concentration (~0.6 mM) and the relationship Mg^{2+}/Ca^{2+} (0.2 ± 0.1) of Tunuyán River suggest dolomite weathering is less important than that of calcite in carbonate dynamics (Smolders *et al.*, 2004). Concentrations are about midway between those of Patagonian Andean rivers (~41°S–71°W) where Mg^{2+} hardly exceeds 0.05 mM (Pedrozo and Chillrud, 1998) and those of River Pilcomayo (~22°S–62°W), with an average value of

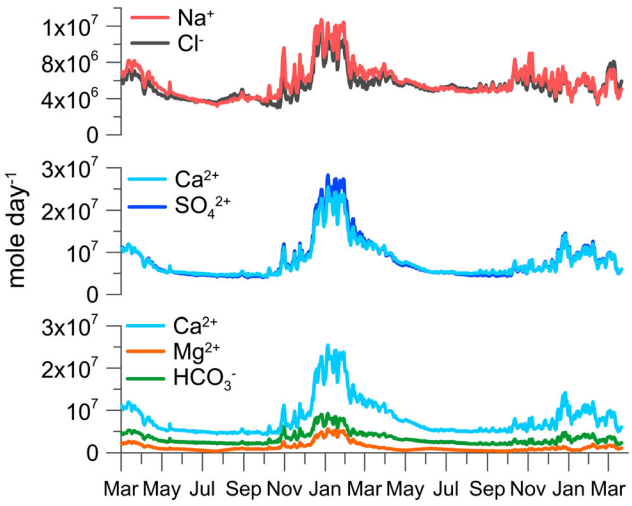

Figure 8. Daily flux (mol day^{-1}) of major ions in Tunuyán River from 2009 to 2011. Ions are grouped by evaporite and carbonate minerals: halite (NaCl) and gypsum ($CaSO_4 \cdot 2H_2O$) and calcite ($CaCO_3$) and dolomite ($CaMg(CO_3)_2$)

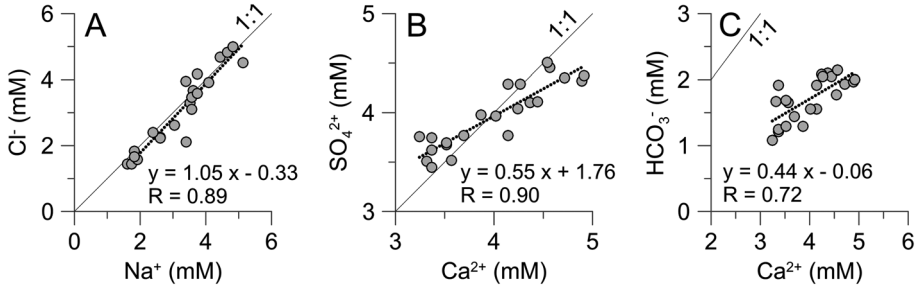

Figure 7. Molar ratios (mM) between major ions in Tunuyán River. The solid line represents the theoretical ratio of (A) halite (NaCl), (B) anhydrite ($CaSO_4$) and (C) ½ calcite ($CaCO_3$)

1.5 mM and Mg^{2+}/Ca^{2+} ratio close to 1 (Smolders *et al.*, 2004). Another source of this ion could be the pyroxene weathering of the crystalline basement of the Frontal Cordillera (Ramos *et al.*, 2010), also found in SPM (Table V), and given its high relative weathering potential in the Goldich dissolution series, it may be considered as a Mg^{2+} source (Meybeck, 2003).

Marine gypsum deposits usually have halite as accessory mineral (Boggs, 2009). In Tunuyán River, the molar concentrations of Na^+ and Cl^- are similar to the expected ones for stoichiometric relationship 1:1 of halite dissolution (Figure 7A), suggesting that this mineral is the major source of Na^+ and Cl^- (Négrel *et al.*, 2007; Ollivier *et al.*, 2010). Nevertheless, some Na^+ remaining is observed (Na^+–$Cl^- = 0.7 \pm 0.1$ mM), which would have additional origins such as other evaporite dissolution like mirabilite [$Na_2SO_4 \cdot 10\ H_2O$ (Skidmore *et al.*, 2010)], sodium silicate weathering (Meybeck, 1987) and cation exchange between Ca^{2+} and Na^+ in shale weathering (Cerling *et al.*, 1989), which are abundant in the basin (Ramos *et al.*, 2010).

Given the spatial evolution of the lithological and geochemical characteristics of the basin, there may be a gradient of factors controlling river geochemistry: a spatial sequence of pyrite weathering to gypsum weathering. The pyrite control weathering would be exercised by the weathering of black shales (largely covered by glaciers), whereas the gypsum control weathering would be due to the presence of evaporite rocks in the middle part of the basin (Figure 1). In current conditions, the pyrite-gypsum weathering balance along the basin responds mostly to lithological differences rather than to precipitation, because, unlike lithology, snow precipitation and melting are somehow uniform throughout the catchment. A significant known factor influencing pyrite weathering is glacier cover (Tranter *et al.*, 2002), which in the future could decrease its effect on river geochemistry owing to the observed and projected glacier retreat (Bradley *et al.*, 2006). In mountain basins, intense hydrological dynamics and low temperature produce high physical erosion rates but low chemical weathering rates (Anderson, 2007; Maher, 2011).

Also, it has been observed that in glacierized basins, SiO_2 weathering rate is lower than that in non-glacierized basins (Anderson, 2007), a fact attributed to low temperatures depressing silicate hydrolysis. The SiO_2 concentration in Tunuyán River (~200 μmol l^{-1}) is similar to that in non-glacial granite basins (~165 μmol l^{-1}: Oliva *et al.*, 2003), and the estimated SiO_2 weathering rate (~3.3 t km^{-2} $year^{-1}$) is close to that of rivers with similar specific discharge with no silicate depression driven by low temperature (~3.0 t km^{-2} $year^{-1}$: Anderson, 2007). Dissolved SiO_2 originates from silicate weathering (Drever, 1997) and from amorphous SiO_2 dissolution present in marine sedimentary rocks (Bluth and Kump, 1994; Clow and Mast, 2010) widely distributed in the Upper Tunuyán River basin (Ramos *et al.*, 2010).

According to Stallard (1995), in mountainous regions, physical erosion is strong enough for K^+-bearing and Mg^{2+}-bearing minerals to be preferentially eroded compared with that for Na^+-bearing and Ca^{2+}-bearing minerals, which are removed prior to physical erosion. Tunuyán River SPM mineralogy showed clays and Al and Fe oxy-hydroxides to account for 5% and 1%, respectively, which are weathering products of feldspar, the most abundant mineral in the basin (Ramos *et al.*, 2010). On the other hand, plagioclase and pyroxene accounted for more than 50%, suggesting that silicate weathering would be occurring at low rates.

Tunuyán River geochemistry shows a strong relationship with Q. Throughout the period under evaluation, water was Ca^{2+}–SO_4^{2-} type. Nevertheless, a reduction in the dominance of these ions was registered during the low Q period, when the water was more concentrated and the ion pair Na^+–Cl^- was more important. River water was oversaturated with respect to calcite all year round and to dolomite during autumn and spring (Figure 4), indicating that calcium salts concentration are available, but its solubility depends on the saturation of the minerals originating them (Meybeck, 1987), generating a buffer system that maintains Ca^{2+}, Mg^{2+} and SO_4^{2-} concentrations within relatively constant levels. This apparent chemostasis has been discussed by Godsey *et al.* (2009) and Clow and Mast (2010). They stated that the slopes of the relationships between concentration (C) and Q (log$C$–logQ) have a physical interpretation: A slope of zero indicates the catchment behaves chemostatically (i.e. the system keeps C constant as Q varies); and a -1 slope would indicate that C varies inversely with Q, as it might be expected if dilution was the dominant process controlling C, such that approximately constant fluxes of solutes were diluted by variable fluxes of water. The slope values for Tunuyán River log$C$–log$Q$ relationships (Table VIII) suggest that Ca^{2+}, Mg^{2+} and SO_4^{2-} have a trend to chemostatical behaviour, which may be produced by the high rock availability and the release of subglacier weathering-products input. On the other hand, K^+, Na^+ and Cl^- showed slopes closer to -1, and therefore, its concentrations would be controlled by a fixed mass of solutes diluted or concentrated by a variable flux of water. Contrary to observations in granitic catchments by Godsey *et al.* (2009), dissolved SiO_2 in Tunuyán River (only for 2010–2011 year) also showed dilution–concentration behaviour, suggesting that summer low SiO_2 C would result from amorphous silica dissolution present in carbonates, evaporites and black shales (this latter rock type is represented by Tunuyán

glacier outflow) diluted by snowmelting. During winter, high SiO_2 C would be the result of poorly diluted, high-transit time-subsurface contribution enriched in silicate weathering products. The chemostatic behaviour was related to annual runoff as steeper slopes were registered during the dry year (Table IX), indicating a weaker buffer capacity for concentration during low discharge scenarios.

The seasonality of Q was reflected in intra-annual dynamics of particulate and dissolved matter loads. Summer high Q is controlled by snowmelt surface inputs of low TDS and high SPM and by concentered subglacier contributions, whereas low winter Q is mainly fed by high TDS–low SPM water from subsurface flux with higher transit time in the catchment (Figures 2, 3 and 7). The higher proportion of SPM flux registered during snow-melting season (~90%) is produced by the positive association between Q and SPM concentrations, which produces an exponential SPM flux increase. On the other hand, as TDS concentration decreases with increasing Q, a lesser proportion of TDS annual flux occurs during the snow-melting season (60%). When comparing an average hydrologic year with a dry one, it is observed that TDS and SPM concentration relationships with Q are steeper (Figure 5), suggesting an 'inter-annual anti-clockwise hysteresis behavior' of these variables because the higher values were recorded during decreasing discharge scenarios.

In Tunuyán River, the TDS export rate (256 t km^{-2} year^{-1}) is higher than that of other evaporitic basins (Table X). This rate is one of the highest in the world when compared with Meybeck and Ragu's data (1996). Similarly, the cation export rate (70 t km^{-2} year^{-1}) is at least three times higher than that of glacierized or non-glacierized granitic basins (1–20 t km^{-2} year^{-1}) (Anderson, 2007). This is due to the steep slopes in the basin topography, the sedimentary lithology, the strong seasonality of atmospheric precipitations and discharge and probably the glacier mechanical effect on rocks (Anderson *et al.*, 1997).

Physical and chemical erosion intensity in Tunuyán River shows an uncoupled seasonal behaviour. During summer, high discharge produces highest SPM concentration and lowest silicate weathering rates, resembling a 'weathering limited' regime (*sensu* Stallard and Edmond, 1983). Conversely, during winter, the discharge is lowest as well as SPM concentration, while TDS concentration and silicate weathering rates are higher, approximating to a 'transport limited' regime. This shift suggests that Tunuyán River water composition is controlled by snow/glacier melting in summer and by groundwater recharge during winter.

Table IX. Linear regression slopes between solutes concentration and discharge for whole studied period (2009–2011), for the average discharge year (2009–2010) and for the dry year (2010–2011)

Period	Ca^{2+}	Na^{+}	Mg^{2+}	K^{+}	SO_4^{2-}	HCO_3^{-}	Cl^{-}	SiO_2
2009–2011	−0.19	−0.59	0.02	−0.53	−0.09	−0.34	−0.68	—
2009–2010	−0.14	−0.45	0.03	−0.63	−0.05	−0.33	−0.53	—
2010–2011	−0.24	−0.94	−0.28	−0.44	−0.14	−0.44	−0.98	−0.69

Values close to −1 would indicate dilution/concentration behaviour, and values close to 0 would indicate chemostatic behaviour.

Table X. Total dissolved solids (TDS) export rate comparison in rivers of different lithology, presence of glaciers and specific discharge

River	Area (km^2)	Lithology	Glaciers	Runoff (m year^{-1})	TDS export rate (t km^{-2} year^{-1})	Reference
Tunuyán	2830	Mixed evaporitic	x	0.32	256	This study
Wujiang	66 849	Mixed carbonatic		0.56	198	Han and Liu (2004)
Rhöne	98 800	Mixed carbonatic	x	0.57	178	Ollivier *et al.* (2010)
Ebro	85 530	Mixed evaporitic		0.06	70	Négrel *et al.* (2007)
Upper Manso	169	Granitic	x	2.24	57	Pedrozo and Chillrud (1998)
Glacier outlet	28	Granitic	x	8.02	268	Pedrozo and Chillrud (1998)
Huai	270 000	Mixed carbonatic		0.23	49	Zhang *et al.* (2011)
Pilcomayo	98 500	Mixed carbonatic		0.07	46	Smolders *et al.* (2004)
Bermejo	123 000	Mixed carbonatic		0.11	41	Pedrozo and Bonetto (1987)
Agua Negra	240	Volcanic	x	0.39	17	Lecomte *et al.* (2008)
San José	200	Granitic		0.07	15	Lecomte *et al.* (2011)
Dammareuss	11	Granitic	x	2.71	15	Hindshaw *et al.* (2011)

CONCLUSIONS

This study constitutes one of the first assessments of physical and chemical erosion in a mountain river in pristine conditions where evaporite lithology and the presence of glaciers are combined. Samples of water, snow and sediments were analysed over a period of 2 years under different hydrological conditions (2009–2010, $Q_{avg} = 100\%$ and 2010–2011, $Q_{avg} = 60\%$).

The seasonal variations in the Tunuyán River discharge responded to snowpack dynamics and were associated to the [SPM] and [TDS] through positive and negative power relationships, respectively. Water was highly mineralized (9.6–15.5 meq l^{-1}) with high concentrations of Ca^{2+} and SO_4^{2-} (~4 mmol l^{-1}), indicating the influence of lithology on river chemistry. The analyses of the relationships between major cations and anions suggest that river geochemistry is mainly governed by evaporite dissolution ($CaSO_4$ and NaCl), pyrite (FeS_2) oxidation and carbonate weathering and, to a lesser degree, silicate weathering and atmospheric inputs.

Throughout the period under evaluation, the geochemistry of snow precipitations in the eastern slope of the Andes showed a distinct continental influence ($Na^+/Ca^{2+} = 0.17$). The atmospheric input of dissolved solids to Tunuyán River was estimated to be lower than 1% (by mass).

We observed that 92% to 86% of SPM and 67% to 54% of TDS annual transport take place during the high discharge snow-melting season. The inter-annual variability of SPM and TDS loads were directly related to discharge, which had a more significant effect over particulate matter transport. SPM and TDS loads for the average discharge year (2009–2010) were estimated to be 1.19 and 0.68×10^6 t $year^{-1}$, respectively. During the dry year (2010–2011), we observed a decrease in SPM and TDS loads of 35% (0.79×10^6 t $year^{-1}$) and 19% (0.55×10^6 t $year^{-1}$), respectively.

The high solubility of the minerals that form the rocks of Tunuyán River basin (evaporites, carbonates and black shales) and the mechanical action of the glaciers located in the high catchment would be the factors producing the high solute export rates observed. TDS weathering rates estimated in this study were higher than those observed in glacierized granite basins and in non-glacierized evaporite basins, suggesting a synergistic effect of lithology and glaciers on physical and chemical weathering in this mountain river.

ACKNOWLEDGEMENTS

This study received financial support from ANPCyT (PICT 2010-0270), Universidad Nacional del Comahue (Program 04/B166). The authors thank P. Bueno for the chemical analyses and lab assistance; H. Segal and A. Villodas for hydrologic data and discussion; K. Lecomte and E. Freguglia for the geological and hydrochemical data discussion; L. Ferri and P. Pitte for the glacier data and mapping assistance; and R. Aguilar for the English review. We also wish to thank two anonymous reviewers whose comments and suggestions greatly improved the original manuscript.

REFERENCES

Anderson SP, Drever JI, Humphrey NF. 1997. Chemical weathering in glacial environments. *Geology* **25**(5): 399–402.

Anderson SP. 2007. Biogeochemistry of glacial landscape systems. *Annual Review of Earth and Planetary Sciences* **35**: 375–399.

APHA. 1998. *Standard Methods for the Examination of Water and Wastewater*, 20th edn. American Public Health Association: Washington; 1325.

Barry RG, Chorley R. 2010. *Atmosphere, Weather and Climate*. Routledge: London; 516 pp.

Bluth GJS, Kump LR. 1994. Lithologic and climatologic controls of river chemistry. *Geochimica et Cosmochimica Acta* **58**: 2341–2359.

Boggs S. 2009. *Petrology of Sedimentary Rocks*. Cambridge University Press: Cambridge; 600.

Bradley RS, Vuille M, Diaz HF, Vergara W. 2006. Threats to water supplies in the tropical Andes. *Science* **312**: 1755–1756.

Cerling TE, Pederson BL, Von Damm KL. 1989. Sodium–calcium ion exchange in the weathering of shales: implications for global weathering budgets. *Geology* **17**(6): 552–554.

Chambouleyron J, Salatino S, Morabito J, Fornero L. 1993. Performance of basin irrigation in the Lower Tunuyán River in Mendoza, Argentina. *Irrigation and Drainage Systems* **7**(1): 1–11.

Clow DW, MA Mast. 2010. Mechanisms for chemostatic behavior in catchments: implications for CO_2 consumption by mineral weathering. *Chemical Geology* **269**: 40–51.

De Walle DR, Rango A. 2008. *Principles of Snow Hydrology*. Cambridge University Press: Cambridge; 410.

Depetris PJ, Gaiero DM, Probst JL, Hartmann J, Kempe S. 2005. Biogeochemical output and typology of rivers draining Patagonia's Atlantic seaboard. *Journal of Coastal Research* **21**(4): 835–844.

DGI (Departamento General de Irrigación). 2011. *Runoff Forecast for the Rivers Mendoza, Tunuyán, Diamante, Malargüe and Grande*. In Spanish. Departamento General de Irrigación: Mendoza; 18.

Drago E, Quirós R. 1996. The hydrochemistry of the inland waters of Argentina; a review. *International Journal of Salt Lake Research* **4**: 315–325.

Drever JI. 1997. *The Geochemistry of Natural Waters*. Prentice Hall: New Jersey; 436.

Gaillardet J, Dupré B, Louvat P, Allègre CJ. 1999. Global silicate weathering and CO_2 consumption rates deduced from the chemistry of large rivers. *Chemical Geology* **159**: 3–30.

Gibbs RJ. 1970. Mechanisms controlling world water chemistry. *Science* **170**: 1088–1090.

Godsey SE, Kirchner JW, Clow DW. 2009. Concentration–discharge relationships reflect chemostatic characteristics of catchments. *Hydrological Processes* **23**: 1844–1864.

Godsey SE, Kirchner JW, Tague CL. 2013. Effects of changes in winter snowpacks on summer low flows: case studies in the Sierra Nevada, California, USA. *Hydrological Processes*. DOI: 10.1002/hyp.9943

Gustafsson JP. 2010. Visual MINTEQ version 3.0. *KTH Royal Inst. of Technol., Stockholm, Sweden*.

Hall DK, GA Riggs, VV Salomonson. 2011, updated daily. MODIS/Terra Snow Cover Daily L3 Global 0.05Deg CMG V004, June to September 2009 and September to October 2010. National Snow and Ice Data Center: Boulder; Digital media.

Han G, Liu C. 2004. Water geochemistry controlled by carbonate dissolution: a study of the river waters draining karst-dominated terrain, Guizhou Province, China. *Chemical Geology* **204**: 1–21.

Hindshaw RS, Tipper ET, Reynolds BC, Lemarchand E, Wiederhold JG, Magnusson J, Bernasconi SM, Kretzschmar R, Bourdon B. 2011.

Hydrological control of stream water chemistry in a glacial catchment (Damma Glacier, Switzerland). *Chemical Geology* **285**(1): 215–230.

Hoke GD, Aranibar JN, Viale M, Araneo DC, Llano C. 2013. Seasonal moisture sources and the isotopic composition of precipitation, rivers, and carbonates across the Andes at 32.5–35.5°S. *Geochemistry, Geophysics, Geosystems* **14**: 962–978.

IANIGLA-Inventario Nacional de Glaciares. In press. Subcuencas de los ríos Palomares, Salinillas, Colorado, cajón río Tunuyán y arroyo San Carlos, cuenca del río Tunuyán, Provincia de Mendoza. IANIGLA-CONICET, Secretaría de Ambiente y Desarrollo Sustentable de la Nación: Buenos Aires; 55.

Immerzeel WW, van Beek LP, Bierkens MF. 2010. Climate change will affect the Asian water towers. *Science* **328**(5984): 1382–1385.

Kay SM, Mpodozis C, Ramos VA. 2004. Andes. In *Encyclopedia of Geology* vol. **1**, Selley RC, Cocks LR, Plimer IR (eds). Academic Press: Amsterdam; 118–131.

Krnavek L, Simpson WR, Carlson D, Domine F, Douglas TA, Sturm M. 2012. The chemical composition of surface snow in the Arctic: examining marine, terrestrial, and atmospheric influences. *Atmospheric Environment* **50**: 349–359.

Kump LR, Brantley SL, Arthur MA. 2000. Chemical weathering, atmospheric CO_2, and climate. *Annual Review of Earth and Planetary Sciences* **28**: 611–667.

Langmuir D. 1997. *Environmental Geochemistry*. Prentice Hall: New Jersey; 600.

Lasaga AC, Soler JM, Ganor J, Burch TE, Nagy KL. 1994. Chemical weathering rate laws and global geochemical cycles. *Geochimica et Cosmochimica Acta* **58**: 2361–2386.

Lecomte KL, Milana JP, Formica SM, Depetris PJ. 2008. Hydrochemical appraisal of ice and rock-glacier meltwater in the hyperarid Agua Negra drainage basin, Andes of Argentina. *Hydrological Processes* **22**: 2180–2195.

Lecomte KL, García MG, Fórmica SM, Depetris PJ. 2011. Hidroquímica de ríos de montaña (sierras de córdoba, Argentina): elementos mayoritarios disueltos. *Latin American Journal of Sedimentology and Basin Analysis* **18**(1): 43–62.

Liu ZH, Zhao J. 2000. Contribution of carbonate rock weathering to the atmospheric CO_2 sink. *Environmental Geology* **39**: 1053–1058.

Maher K. 2011. The role of fluid residence time and topographic scales in determining chemical fluxes from landscapes. *Earth and Planetary Science Letters* **312**: 48–58.

Manzur A, León JG, Peralta PI, Romay C, Basile JC, Lorenzo FE, Méndez ME, Arias A, Pereira R. 2006. *Characterization of the surface hidric system of Mendoza province*. Technical report (final). In spanish. Departamento General de Irrigación, PROSAP-OEI. Mendoza. 176.

Masiokas HM, Villalba R, Luckman BH, Le Quesne C, Aravena JC. 2006. Snowpack variations in the Central Andes of Argentina and Chile, 1951–2005: large-scale atmospheric influences and implications for water resources in the region. *Journal of Climate* **19**: 6334–6352.

Masiokas MH, Villalba R, Luckman BH, Mauget S. 2010. Intra-to multidecadal variations of snowpack and streamflow records in the Andes of Chile and Argentina between 30 and 37 S. *Journal of Hydrometeorology* **11**(3): 822–831.

McDonnell JJ, McGuire K, Aggarwal P, Beven KJ, Biondi D, Destouni G, Dunn S, James A, Kirchner J, Kraft P, Lyon S, Maloszewski P, Newman B, Pfister L, Rinaldo A, Rodhe A, Sayama T, Seibert J, Solomon K, Soulsby C, Stewart M, Tetzlaff D, Tobin C, Troch P, Weiler M, Western A, Wörman A, Wrede S. 2010. How old is streamwater? Open questions in catchment transit time conceptualization, modelling and analysis. *Hydrological Processes* **24**: 1745–1754.

Meybeck M. 1987. Global chemical weathering of surficial rocks estimated from river dissolved loads. *American Journal of Science* **287**: 401–428.

Meybeck M. 2003. Global occurrence of major elements in rivers. In *Treatise on Geochemistry* vol. **5**, JI Drever (ed). Elsevier: Amsterdam; 207–224.

Meybeck M, Ragu A. 1996. River discharge to the oceans: an assessment of suspended solids, major ions, and nutrients. UNEP/WHO, Environment of Information and Assessment Div.: Nairobi; 245.

Mitchell AC, Lafrenière MJ, Skidmore ML, Boyd ES. 2013. Influence of bedrock mineral composition on microbial diversity in a subglacial environment. *Geology* **45**: 855–858.

Moatar F, Meybeck M. 2005. Compared performances of different algorithms for estimating annual nutrient loads discharged by the eutrophic River Loire. *Hydrological Processes* **19**(2): 429–444.

Montross SN, Skidmore M, Tranter M, Kivimäki AL, Parkes RJ. 2013. A microbial driver of chemical weathering in glaciated systems. *Geology* **41**(2): 215–218.

Négrel P, Roy S, Petelet-Giraud E, Millot R, Brenot A. 2007. Long-term fluxes of dissolved and suspended matter in the Ebro River Basin (Spain). *Journal of Hydrology* **342**: 249–260.

O'Brien NR, Slatt RM. 1990. *Argillaceous Rock Atlas*. Springer-Verlag: New York; 139.

Oliva P, Viers J, Dupré B. 2003. Chemical weathering in granitic environments. *Chemical Geology* **202**: 225–256.

Ollivier P, Hamelin B, Radakovitch O. 2010. Seasonal variations of physical and chemical erosion: a three-year survey of the Rhone River (France). *Geochimica et Cosmochimica Acta* **74**: 907–927.

Pedrozo FL, Bonetto CA. 1987. Nitrogen and phosphorus transport in the Bermejo River (South America). *Revue D'Hydrobiologie Tropicale* **20**(2): 91–99.

Pedrozo FL, Chillrud SN. 1998. Relative water fluxes and silicate weathering from the tributaries of a small glaciated watershed in the southern Patagonian Andes (Upper Manso watershed, Argentina). *Verhandlungen Internationale Vereines Limnologie* **26**: 935–939.

Pedrozo F, Chillrud S, Temporetti P, Diaz M. 1993. Chemical Composition and nutrient limitation in rivers and lakes of Northern Patagonian Andes (39.5°–42°S; 71°W) (Rep. Argentina). *Verhandlungen Internationale Vereines Limnologie* **25**: 207–214.

Ramos VA, Aguirre Urreta MB, Alvarez PP, Coluccia A, Giambiagi LB, Pérez D, Tunik M, Vujovich G. 2010. *Geologic Sheet 3369-III Cerro Tupungato (1: 250.000)*. In Spanish. SGeMAr. Instituto de Geología y Recursos Minerales: Buenos Aires; 133.

Roig FA, Abraham EM, Méndez E. 2007. Vegetation belts, cold and soil freezing in the Central Andes of Mendoza, Argentina. *Phytocoenologia* **37**(1): 99–114.

Schrott L. 1998. The hydrological significance of high mountain permafrost and its relation to solar radiation. A case study in the high Andes of San Juan, Argentina. *Bamberger Geographische Schriften* **15**: 71–84.

Simmers I. 2003. Hydrological processes and water resources management. In *Understanding Water in a Dry Environment*, Simmers I (ed). Taylor and Francis: London; 341.

Skarbøvik E, Stålnacke P, Bogen J, Bønsnes TE. 2012. Impact of sampling frequency on mean concentrations and estimated loads of suspended sediment in a Norwegian river: implications for water management. *Science of the Total Environment* **433**: 462–471.

Skidmore M, Tranter M, Tulaczyk S, Lanoil B. 2010. Hydrochemistry of ice stream beds – evaporitic or microbial effects?. *Hydrological Processes* **24**: 517–523.

Smolders AJP, Hudson-Edwards KA, Van der Velde G, Roelofs JGM. 2004. Controls on water chemistry of the Pilcomayo River (Bolivia, South-America). *Applied Geochemistry* **19**: 1745–1758.

SRH (Subsecretaría de Recursos Hídricos). 2013. *National System of Hydric Information*. In Spanish. Presidencia de la Nación: Buenos Aires; Online data: http://www.hidricosargentina.gov.ar/sistema_sistema.php (Accessed March 2013).

Stallard RF. 1995. Tectonic, environmental, and human aspects of weathering and erosion: a global review from a steady-state perspective. *Annual Review of Earth and Planetary Sciences* **23**: 11–40.

Stallard RF, Edmond JM. 1983. Geochemistry of the Amazon: 2. The influence of geology and weathering environment on the dissolved load. *Journal of Geophysical Research* **88**(14): 9671–9688.

Torres MA, West AJ, Li G. 2014. Sulphide oxidation and carbonate dissolution as a source of CO_2 over geological timescales. *Nature* **507**: 346–349.

Tranter M. 2011. Solute in glacial meltwater. In *Encyclopedia of Snow, Ice and Glaciers*, Singh VP, Singh P, Haritashya UK (eds.). Springer: Dordrecht; 332–341.

Tranter M, Sharp MJ, Lamb HR, Brown GH, Hubbard BP, Willis IC. 2002. Geochemical weathering at the bed of Haut Glacier d'Arolla, Switzerland – a new model. *Hydrological Processes* **16**(5): 959–993.

Urrutia R, Vuille M. 2009. Climate change projections for the tropical Andes using a regional climate model: temperature and precipitation simulations for the end of the 21st century. *Journal of Geophysical Research* **114**: 1–15.

Viale M, Nuñez MN. 2011. Climatology of winter orographic precipitation over the subtropical central Andes and associated synoptic and regional characteristics. *Journal of Hydrometeorology* **12**: 481–507.

Vicuña S, Garreaud R, McPhee J. 2010. Climate change impacts on the hydrology of snowmelt driven basin in semiarid Chile. *Climatic Change* **105**: 469–488.

Viviroli D, Archer DR, Buytaert W, Fowler HJ, Greenwood GB, Hamlet AF, Huang Y, Koboltschnig G, Litaor MI, López-Moreno JI, Lorentz S, Schädler B, Schreier H, Schwaiger K, Vuille M, Woods R. 2011. Climate change and mountain water resources: overview and recommendations for research, management and policy. *Hydrology and Earth System Sciences* **15**: 471–504.

Viviroli D, Dürr HH, Messerli B, Meybeck M, Weingartner R. 2007. Mountains of the world, water towers for humanity: typology, mapping, and global significance. *Water Resources Research* **43**(7): 1–13.

Willis IC. 2011. Rating curve. In *Encyclopedia of Snow, Ice and Glaciers*, Singh VP, Singh P, Haritashya UK (eds.). Springer: Dordrecht; 918–922.

Zhang L, Song X, Xia J, Yuan R, Zhang Y, Liu X, Han D. 2011. Major element chemistry of the Huai River basin, China. *Applied Geochemistry* **26**(3): 293–300.